Computers and Mathematics with Applications 108 (2022) 109–122

Contents lists available at ScienceDirect

Computers and Mathematics with Applications

www.elsevier.com/locate/camwa

A projection scheme for phase change problems with convection ☆

M. El Haddad [a,*], Y. Belhamadia [b], J. Deteix [a], D. Yakoubi [c,a]

[a] Groupe Interdisciplinaire de Recherche en Éléments Finis de l'Université Laval, Département de Mathématiques et Statistiques, Université Laval, Québec, Canada
[b] Department of Mathematics and Statistics, American University of Sharjah, Sharjah, United Arab Emirates
[c] Léonard de Vinci Pôle Universitaire, Research Center, 92 916 Paris La Défense, France

ARTICLE INFO

Keywords:
Phase change
Natural convection
Enthalpy-porosity
Finite elements
Coupled projection

ABSTRACT

Numerical modeling of phase change problems with convection is known to be computationally expensive. The main challenge comes from the coupling between Navier–Stokes and heat energy equations. In this paper, we develop a new scheme for phase change problems based on a projection method. The proposed method reduces the size of the system by splitting the temperature, the velocity, and the pressure fields while preserving the accuracy of the simulations. A single-domain approach using a variant of the enthalpy-porosity formulation is employed. Incompressible Navier–Stokes problem with Boussinesq approximation for thermal effects in solid and liquid regions is considered. We regularize the discontinuous variables such as latent heat and material properties by a continuous and differentiable hyperbolic tangent function. The robustness and effectiveness of the proposed scheme are illustrated by comparing the numerical results with numerical and experimental benchmark.

1. Introduction

Numerical modeling of solid-liquid phase change problems have gained interest over the years and is relevant to many natural and industrial applications such as ice-ocean coupling in earth's climate, mould casting in metal processing, ceramics and polymers industries, solar and thermal energy storage, etc. Several difficulties are encountered in designing efficient and robust models for these types of problems. Among the main challenges one faces is, the evolution of the interface position between the solid and liquid phases, the jump of the physical and thermodynamic properties over the interface, the strong coupling between the fluid motion and the heat transport due to the balance laws of mass, momentum and energy. In addition, phase change problems are computationally expensive, accurate numerical simulations require very fine meshes and small time steps together with appropriate numerical schemes, see for instance [20,48] and the references therein.

Two main approaches exist in the literature to model the evolution of the liquid-solid interface in phase-change problems: The multi-domain approach and the single domain approach. The first approach considers solving the liquid problem and the solid one in two different moving grids. This requires updating the domains at each time step which makes it difficult to track solid-liquid interfaces with complex geometries and structures (see [30,21] and [46]). The second approach uses a single domain for the resolution of the mass, momentum and energy laws in both the solid and liquid phases by means of a semi-phase-field method or enthalpy method (see [49,11,12,38], and [6]). The attractive feature about this approach is that the system of momentum and energy equations is solved in the entire physical domain making the extension to three dimensional applications feasible. For this approach, one needs to solve the Navier–Stokes system of equations in the liquid phase and set the velocity to zero in the solid region. This can be done either by a variable viscosity method [49] or by a penalty source term method [11]. The first method sets the viscosity artificially to very large values in the solid region, which might cause numerical inconsistencies and consequently blow up the solution. The second method is more appropriate, where it imposes a null velocity in the solid region by adding a source term to the momentum equation. This approach may consider the fluid flow in the mushy zone as fluid flow through a porous medium using for instance the Carman-Kozeny penalty term. The reader is referred to [42], where a recent review about mathematical formulations for solid-liquid problems is presented.

☆ This work was supported by the Natural Sciences and Engineering Research Council of Canada (NSERC) Discovery Grant # RGPIN-2015-04932 (J. Deteix).
* Corresponding author.
E-mail addresses: melhadda@giref.ulaval.ca (M. El Haddad), ybelhamadia@aus.edu (Y. Belhamadia), jean.deteix@mat.ulaval.ca (J. Deteix), driss.yakoubi@devinci.fr (D. Yakoubi).

https://doi.org/10.1016/j.camwa.2022.01.001
Received 25 January 2021; Received in revised form 2 December 2021; Accepted 3 January 2022
Available online 18 January 2022

For both approaches of mathematical models, the numerical simulations are challenging and computationally expensive. Capturing accurately the evolution of the moving interface requires fine meshes and small time steps leading to large computational time and memory consumption. The effects of grid size and numerical schemes for solving phase change problems with convection have been reported in many papers including [19], [41], and [31]. It is also shown that second-order accuracy in time and space is required for these types of problems. To overcome these difficulties, mesh adaptation techniques have been recently introduced, where the spatial mesh elements are refined along the interface and flow structure (see [15], [52], and [3] and the references therein). Despite these developments, the numerical simulation is still challenging, especially when dealing with three dimensional real applications. The main computational cost comes from the coupling between Navier–Stokes equations and heat energy equation. For solid-liquid phase change problems with convection, most of the contributions use a mixed formulation where velocity, pressure and temperature are coupled ([53], [39] and [40]), or a decoupled mixed formation where the velocity and pressure are coupled and connected to the diffusion equations via an extrapolation technique [3]. While these methods are numerically very efficient, they are computationally expensive and are almost impossible to use for the three dimensional simulations.

A remedy for such problems is to decouple the unknowns of the problems. Not only decoupling the energy equation from the momentum equation but also one may split the incomprehensibility constraint from the diffusion operator in the Navier–Stokes problem using the Helmoltz decomposition. Operator splitting approaches were introduced by Chorin [13,14] and Temam [44,45] called also the projection methods. These methods are known to be economical for the computational costs and memory requirements. The idea is to solve a sequence of decoupled elliptical problems for the velocity field and the pressure respectively instead of a saddle point Navier–Stokes problem. The method owns some imperfections that were addressed during the years such as the artificial boundary layers of the pressure. This affects the accuracy of the pressure in the schemes and causes artificial boundary layer phenomena next to the interface. Numerical schemes for correcting these defects were studied and analyzed in the literature namely the incremental and the rotational incremental pressure-correction schemes (see [29] for an overview about these schemes). For the coupling between Navier–Stokes and heat equation, a basic projection scheme where the velocity and temperature are decoupled was presented in [27] and [36]. Recently, a coupled projection scheme suitable for thermal-Navier–Stokes coupling was introduced in [16,17]. This method couples the velocity and temperature and the fixed-point loop is reduced to a bare minimum producing accurate numerical solutions, while reducing the computational time.

The main goal of this paper is to develop an original approach based on the projection method suitable for solid-liquid phase change problems with convection. To our knowledge no previous contribution has been reported in the literature using a finite element projection method for these types of problems. The developed method is of second order in time and is inspired from the coupled projection schemes presented in [16] for the thermal-Navier–Stokes equations. The main advantage of the proposed methods is to reduce the size of the system compared to the mixed formulation leading to a reduction in the computational costs and memory requirements, while preserving the accuracy of the numerical solutions. The performance of the proposed scheme is illustrated on melting and solidification benchmark problems and comparison with existing experimental and numerical results found in the literature is performed as well.

The outline of the paper is as follows: In section 2, we describe the governing equations of the problem as well as the smoothing technique used to model the jump of the physical and thermodynamic properties over the interface. In section 3, we present a second order projection method with pressure and velocity correction, while section 4 is devoted to a validation of the proposed scheme by comparing it to existing numerical simulations and experiments.

2. The mathematical model

In this section, we present the governing system of equations used to model the solid-liquid phase change problem with natural convection. We produce the system in terms of dimensionless quantities and introduce the appropriate space definitions. The time discretization is presented as well.

A purely mathematical strategy makes it possible to model the phase change problem using a single domain and a single set of equations. We assume that both phases (fluid and solid) are determined by a critical temperature, a convection-diffusion model coupled with a Navier-Stokes model which drives the phase change with convection. In this type of formulation, the variation of the physical proprieties between liquid and solid states is considered in the energy equation only. However, an *artificial* penalty term is added to the momentum to take into account both fluid and solid state. Below the critical temperature where a solid state is assumed, the penalty term dominates *forcing the velocity to be null* reducing the momentum equation to a diffusion equation. Above the critical temperature, the penalty term is null and the dynamics is described by the Navier-Stokes and convection-diffusion system.

2.1. Governing equations

We consider a domain $\Omega \in \mathbb{R}^d$, with $d = 2$ or 3. The subscript s will refer to the solid phase and the subscript l will refer to the liquid phase. We denote by $\partial\Omega$ the boundary of the domain Ω which admits a partition without overlap into three parts: Γ_{hot}, Γ_{cold} and Γ_a such that $\partial\Omega = \Gamma_{hot} \cup \Gamma_{cold} \cup \Gamma_a$. We consider a fixed final time $t^\star$ (a positive real number), and the physical time is denoted $\tau \in [0, \tau^\star]$ while $\boldsymbol{X} \in \Omega$ denote the spatial variable.

We assume that the fluid is Newtonian and follow the Boussinesq approximation: all physical parameters are assumed to be constant and the fluid is subject to an external volumetric force which accounts for buoyancy forces (which are null in the solid phase). Therefore, this force F_B is proportional to the variation of the density $\rho(\cdot)$ (expressed generally in terms of temperature T variation with respect to a reference temperature T_{ref}). Note that a linear approximation is often introduced to further simplify the problem.

$$F_B = -g\frac{\rho(T) - \rho(T_{ref})}{\rho(T_{ref})} \approx g\beta(T - T_{ref})$$

where g is the gravity and β account for the thermal expansion.

Remark 1. In certain cases (natural air convection for example) the linear Boussinesq forces are plainly justified, however in problems such as water convection or water freezing the exact expression, generally nonlinear in T, must be used.

Finally, these definitions of F_B are essential to have a coherent physical model for the phase change phenomenon. However, as observed in [16,17] from a numerical standpoint this definition of F_B is not essential to the proposed numerical scheme, a more generic function F_B and even thermal dependency of the viscosity and could be considered. However, for sake of simplicity, in the presentation of the different algorithms, the linear Boussinesq approximation is used.

With the Boussinesq approximation for thermal effect the fluid flow is modeled with the following incompressible Navier–Stokes equations (or Brinkman equations since we have the additional term $A\boldsymbol{U}$):

$$\begin{cases} \dfrac{\partial \boldsymbol{U}}{\partial \tau} + \boldsymbol{U}\cdot\nabla\boldsymbol{U} = \nabla\cdot(2\nu_l \boldsymbol{D}\boldsymbol{U}) - \nabla P + A\boldsymbol{U} + F_B \boldsymbol{e}_d \\ \nabla\cdot\boldsymbol{U} = 0 \end{cases} \tag{1}$$

where $\boldsymbol{U}$ is the velocity, $\boldsymbol{D}\boldsymbol{U} = (\nabla\boldsymbol{U} + \nabla\boldsymbol{U}^T)/2$ is the deformation tensor, P is the pressure, T is the temperature, $\nu_l = \mu_l/\rho_l$ is the kinematic viscosity (μ_l is the dynamic viscosity and ρ_l is the density). $A\boldsymbol{U}$ is the Carman-Kozeny penalty term that is artificially introduced in the momentum equation to impose a null velocity and pressure in the solid region. The function A is defined as follows:

$$A = -c_A \frac{(1-\eta)^2}{\eta^3 + b}$$

where c_A is a constant accounting for the mushy region, η is the porosity and b is a small nonnegative constant ($b = 10^{-6}$) introduced to avoid division by 0. The energy equation is modeled by the enthalpy method as follows:

$$\frac{\partial H}{\partial \tau} + \boldsymbol{U}\cdot\nabla H - \nabla\cdot(k(T)\nabla T) = 0$$

where H is the enthalpy defined by

$$H = \begin{cases} H_s = \rho_s c_s T & \text{if } T < T_f, \\ H_l = \rho_l L + \rho_s c_s T_f + \rho_l c_l (T - T_f) & \text{if } T > T_f \end{cases}$$

and the thermal conductivity

$$k(T) = \begin{cases} k_l & \text{if } T \geq T_f, \\ k_s & \text{if } T < T_f \end{cases}$$

where ρ_i, c_i, and k_i are the density, specific heat and thermal conductivity for each state respectively. In the case of isothermal phase change, as in [4–6], the energy equation based on temperature is given by

$$c(T)\frac{\partial T}{\partial \tau} + c(T)(\boldsymbol{U}\cdot\nabla T) + \frac{\partial s(T)}{\partial \tau} - \nabla\cdot(k(T)\nabla T) = 0. \tag{2}$$

The function s represents the jump of the enthalpy between the solid and liquid regions. It is zero in the solid region and equal to $\rho_l L$ in the liquid where L is the latent heat of fusion. The phase change is assumed to occur in an artificial mushy zone in a small temperature interval $T \in [T_f - \varepsilon, T_f + \varepsilon]$ around the temperature of fusion T_f (where $\varepsilon > 0$ is a small number) and we have

$$c(T) = \begin{cases} \rho_l c_l & \text{if } T \geq T_f \\ \rho_s c_s & \text{if } T < T_f. \end{cases}$$

Obviously for (1) and (2) to be a well posed problem it must be fitted with boundary and initial conditions. Here, for the sake of simplicity, Dirichlet condition will be imposed on the velocity $\boldsymbol{U}$ of the liquid phase and a set of Dirichlet and Neumann condition is imposed on the temperature

$$\boldsymbol{U} = \boldsymbol{0}, \quad \text{on } \partial\Omega, \qquad T = T_{hot}, \quad \text{on } \Gamma_{hot}, \qquad T = T_{cold}, \quad \text{on } \Gamma_{cold}, \qquad \partial_n T = q_a, \quad \text{on } \Gamma_a$$

where $\partial_n T$ is the heat flux. As for initial conditions we will simply note

$$\boldsymbol{U}(\boldsymbol{X}, 0) = \boldsymbol{U}_0(\boldsymbol{X}), \quad \nabla\cdot\boldsymbol{U}_0 = 0, \quad T(\boldsymbol{X}, 0) = T_0(\boldsymbol{X}), \quad \text{in } \Omega.$$

Of course T_{hot}, T_{cold}, q_a, $\boldsymbol{U}_0$ and T_0 are given, and parts of the boundary ($\Gamma_{hot}, \Gamma_{cold}, \Gamma_a$) could be an empty set although recall that $\partial\Omega = \Gamma_{hot} \cup \Gamma_{cold} \cup \Gamma_a$.

2.2. Dimensionless system of equations

We have already introduced T_{ref}, let us introduce some other reference values: L_{ref} for length, ρ_{ref} for density, V_{ref} the reference velocity and δT the difference of temperature applied on the body along the boundary. We define the following nondimensional variables for the space, velocity, temperature and time:

$$\boldsymbol{x} = \frac{\boldsymbol{X}}{L_{ref}}, \; t = \frac{V_{ref}}{L_{ref}}\tau, \; \boldsymbol{u} = \frac{\boldsymbol{U}}{V_{ref}}, \; p = \frac{P}{V_{ref}^2}, \; \theta = \frac{T - T_{ref}}{\delta T}.$$

The Reynold number Re, the Prandtl number Pr and the adimensional external forces are defined as

$$Re = \frac{V_{ref} L_{ref}}{\nu_l}, \quad Pr = \frac{\rho_l c_l \nu_l}{k_l}, \quad f_B(\theta) = \frac{L_{ref}}{V_{ref}^2} F_B(\delta T\theta + T_{ref})$$

and, denoting $\Omega_t = \Omega \times (0, t^*)$, the dimensionless system of equations is written as:

$$\begin{cases} \dfrac{\partial \boldsymbol{u}}{\partial t} + \boldsymbol{u} \cdot \nabla \boldsymbol{u} - \dfrac{2}{Re} \nabla \cdot \boldsymbol{D}\boldsymbol{u} + \nabla p - A(\theta)\boldsymbol{u} = f_B(\theta)\boldsymbol{e}_d & \text{in } \Omega_t, \\ \nabla \cdot \boldsymbol{u} = 0 & \text{in } \Omega_t, \\ C(\theta)\dfrac{\partial \theta}{\partial t} + C(\theta)\boldsymbol{u} \cdot \nabla \theta + \dfrac{\partial S(\theta)}{\partial t} - \nabla \cdot \left(\dfrac{k(\theta)}{RePr} \nabla \theta \right) = 0 & \text{in } \Omega_t, \\ \boldsymbol{u}(\cdot, t)|_{\partial\Omega} = 0 \qquad \theta(\cdot, t)|_{\Gamma_{hot}} = \theta_{hot} \qquad \theta(\cdot, t)|_{\Gamma_{cold}} = \theta_{cold} \qquad \partial_{\boldsymbol{n}} \theta(\cdot, t)|_{\Gamma_a} = h_a & \\ \boldsymbol{u}(\boldsymbol{x}, 0) = \boldsymbol{u}_0(\boldsymbol{x}), \quad \theta(\boldsymbol{x}, 0) = \theta_0(\boldsymbol{x}), & \text{in } \Omega. \end{cases} \tag{3}$$

Where θ_{hot}, θ_{cold}, h_a, $\boldsymbol{u}_0$, θ_0 are the rescaled boundary and initial conditions. From the linear Boussinesq hypothesis the buoyancy force f_B can be explicited. Introducing the Rayleigh number Ra

$$Ra = g\beta\delta T \frac{L_{ref}^3 \rho_l c_l}{\nu_l k_l}, \qquad f_B(\theta) = g\beta\delta T \frac{L_{ref}}{V_{ref}^2}\theta = \frac{Ra}{PrRe^2}\theta.$$

The non-dimensional function S, conductivity and specific heat are defined as:

$$S(\theta) = \frac{s}{s_l} = \begin{cases} \dfrac{L}{c_l \delta T} = \dfrac{1}{Ste} & \text{if } \theta \geq \theta_f, \\ 0 & \text{if } \theta < \theta_f, \end{cases} \tag{4}$$

where Ste is the Stephan number,

$$K(\theta) = \frac{k(\theta)}{k_l RePr} = \begin{cases} 1/(RePr) & \text{if } \theta \geq \theta_f, \\ k_s/(k_l RePr) & \text{if } \theta < \theta_f, \end{cases} \quad \textit{and} \quad C(\theta) = \frac{c}{c_l} = \begin{cases} 1 & \text{if } \theta \geq \theta_f, \\ c_s/c_l & \text{if } \theta < \theta_f. \end{cases}$$

We regularize all liquid-solid step functions, such as S, K, C, using a continuous and differentiable hyperbolic-tangent function F as in [15]. For a quantity $Q(\theta)$ having two states, we redefine (i.e. keeping the same notation) $Q(\theta)$ using the regularized function F:

$$Q(\theta) = F(\theta, q_l, q_s, a_s, \theta_r, R_s) = q_l + \frac{q_s - q_l}{2}\left[1 + \tanh\left(a_s\left(\frac{\theta_r - \theta}{R_s}\right)\right)\right], \tag{5}$$

where q_l, q_s are the imposed values in the liquid and solid regions, θ_r the value around which we regularize and a_s and R_s are smoothing parameters. Both parameters are used to affect the slope of the tangent hyperbolic curve fitting q_l and q_s. The bigger (respectively smaller) the ratio a_s/R_s the steeper (respectively flatter) the curve fitting gets. Therefore a_s/R_s control the thickness of the transition zone. As an example, for a thickness of 0.2 around the reference value $\theta_r = \theta_f$, fixing $R_s = \epsilon = 0.1$ and $a_s = 5$ the function $S(\theta)$ defined as:

$$S(\theta) = F(\theta, \frac{1}{Ste}, 0; 5, \theta_f, \epsilon) = \frac{1}{Ste} - \frac{1}{2Ste}\left[1 + \tanh\left(\frac{\theta_f - \theta}{\epsilon/5}\right)\right],$$

is a regularized version of (4) over the artificial mushy region $[\theta_f - \varepsilon, \theta_f + \varepsilon]$. The enthalpy-porosity term $A(\theta)$ in the momentum equation can be written as

$$A(\theta) = -\frac{C_A(1 - L_f(\theta))^2}{L_f(\theta)^3 + b}, \tag{6}$$

where $L_f(\theta)$ is a regularized Heaviside function (using (5)) defined as 1 in the fluid region and 0 in the solid. L_f defines the liquid fraction inside the artificial mushy-region.

Remark 2. As the objective of this paper is to introduce a new numerical scheme, theoretical considerations will be omitted and treated in a coming paper. Nevertheless, we will consider the following functional setting: we assume

$$\theta_0 \in L^2(\Omega), \qquad \boldsymbol{u}_0 \in \boldsymbol{L}^2(\Omega) \quad \text{with } \nabla \cdot \boldsymbol{u}_0 = 0$$

and

$$\theta_{cold} \in L^2(0, t^*; H^{\frac{1}{2}}(\Gamma_{cold})), \qquad \theta_{hot} \in L^2(0, t^*; H^{\frac{1}{2}}(\Gamma_{hot})), \qquad h_a \in L^2(0, t^*; H_{00}^{\frac{1}{2}}(\Gamma_a)').$$

Therefore we assume

$$\boldsymbol{u} \in L^2(0, t^*; \boldsymbol{H}_0^1(\Omega)), \qquad p \in L^2(0, t^*; L_0^2(\Omega)), \qquad \theta \in L^2(0, t^*; H^1(\Omega)).$$

2.3. Time discretization

Approximation of the time derivative is based on a partition of the adimensional time interval $[0, t^\star]$ into N equal subintervals $[t^n, t^{n+1}]$ for simplicity. The uniform time-step is denoted $\Delta t = t^\star / N$ and $t^n = n\Delta t$ for $n = 0, \cdots, N$.

For $g(\boldsymbol{x}, t)$ we denote by $g^n = g(\boldsymbol{x}, t^n)$ the evaluation of g at times t^n. We denote by D_t the finite difference scheme used to approximate the time derivative of order p:

$$\frac{\partial g(\boldsymbol{x}, t^n)}{\partial t} = \mathcal{D}_t g^n + \mathcal{O}((\Delta t)^p).$$

Introducing the time derivative approximation at time t^{n+1} the fully implicit semi-discrete in time problem (3) can be written as a sequence of problems:

$$\boldsymbol{u}^0 = \boldsymbol{u}_0, \quad \theta^0 = \theta_0, \qquad \text{in } \Omega$$

and at each time step (for $n \geq 0$), we have to solve

$$\begin{cases} \mathcal{D}_t \boldsymbol{u}^{n+1} + \boldsymbol{u}^{n+1} \cdot \nabla \boldsymbol{u}^{n+1} - \dfrac{2}{Re} \nabla \cdot \boldsymbol{D}\boldsymbol{u}^{n+1} + \nabla p^{n+1} - A(\theta^{n+1}) \boldsymbol{u}^{n+1} = f_B(\theta^{n+1}) \boldsymbol{e}_d & \text{in } \Omega, \\ \nabla \cdot \boldsymbol{u}^{n+1} = 0 & \text{in } \Omega, \\ C(\theta^{n+1}) \mathcal{D}_t \theta^{n+1} + C(\theta^{n+1}) \boldsymbol{u}^{n+1} \cdot \nabla \theta^{n+1} + \mathcal{D}_t S(\theta^{n+1}) - \nabla \cdot \left(K(\theta^{n+1}) \nabla \theta^{n+1} \right) = 0 & \text{in } \Omega, \\ \boldsymbol{u}^{n+1}|_{\partial\Omega} = 0 \qquad \theta^{n+1}|_{\Gamma_{hot}} = \theta_{hot} \qquad \theta^{n+1}|_{\Gamma_{cold}} = \theta_{cold} \qquad \partial_{\boldsymbol{n}} \theta^{n+1}|_{\Gamma_a} = h_a. \end{cases} \tag{7}$$

For the sake of simplicity and clarity, the method proposed in this paper will be based on a second order backward time discretization (BDF2 also known as Gear) defined by

$$\mathcal{D}_t g^n = \frac{3g(\boldsymbol{x}, t^n) - 4g(\boldsymbol{x}, t^{n-1}) + g(\boldsymbol{x}, t^{n-2})}{2\Delta t}.$$

Although the rest of this work will be presented using BDF2 *this choice has no effect on our construction*, the methods proposed here could use other (in certain cases more suitable) time schemes. The choice of BDF2 is based on our previous experience in a different type of moving interface problem [2], where BDF2 scheme provided better numerical solutions compared to Crank-Nisolson scheme.

However, for the Navier-Stokes system alone, it is well known that projection methods have an inherent splitting error and a conjectured ceiling of order 2 for the accuracy in H^1 norm. This last observation makes the use of a time discretization of order higher than 2 in the projection pointless; for the Navier-Stokes system alone and a fortiori for (7).

Remark 3. For the BDF2 scheme, the first time step t^1, a simple backward Euler or Crank-Nicolson time step could be used.

3. A coupled projection scheme for phase change problems

In this section, we present a projection scheme for the phase change problems. Splitting the Navier–Stokes equation by the projection method as originally proposed in [13,43] can be a cause of inaccuracy issues (sub-optimal order of the time scheme and non-consistent boundary conditions). In [26], Goda improved the order of the scheme by adding a pressure gradient from the previous step to the velocity prediction problem, producing what is called an *incremental projection method*. Though these schemes were of optimal order for the velocity (in L^2 norm), the pressure was still subject of an artificial boundary condition. In [47], the method was enhanced to produce the *rotational pressure correction projection* which avoids the non-physical boundary condition on the pressure and improves the rate of convergence of the pressure (for a clear overview of this development we refer the reader to [29]). In [16], constructed and analyzed a new method (the *coupled projection scheme* (CPS)) for a Navier–Stokes flows coupled to a convection-diffusion equation. However in their paper they only treated a BDF1 time scheme, used an incremental projection method and more importantly the Carman-Kozeny term (6) was not present in their work. In this work, we propose a extension of the CPS based on a rotational pressure correction with a BDF2 time scheme for the enthalpy-porosity formulation of phase change problems.

In preparation and as a comparison to the proposed coupled projection method, we make a quick review of the basic methods consisting in a fixed point approach to solve (7). Various strategies could be used to address the difficulties related with the nonlinear and coupling terms in (7). Then the convergence of the fixed point (of course, when there is a convergence) would depend on the chosen strategy. We will present in the next two subsections two of those possible strategies.

3.1. Mixed coupled scheme

Obviously starting from the global set of equation, one of the most natural choice consist in applying Newton's method to (7) (this is the method proposed in [15,40]). In that case, at each time step t^{n+1} we apply the following *mixed-coupled algorithm*

1. *Initialization:*

$$\boldsymbol{u}_0 = \boldsymbol{u}^n, \quad p_0 = p^n, \quad \theta_0 = \theta^n \qquad \text{in } \Omega.$$

2. *Determine* $(\boldsymbol{u}^{n+1}, p^{n+1}, \theta^{n+1})$ *as the limit of the fixed point: until convergence, compute* $(\boldsymbol{u}_k, p_k, \theta_k)$ *solution of*

$$
\begin{cases}
\dfrac{3}{2\Delta t}\boldsymbol{u}_k + \boldsymbol{u}_{k-1}\cdot\nabla\boldsymbol{u}_k + \boldsymbol{u}_k\cdot\nabla\boldsymbol{u}_{k-1} - \dfrac{2}{Re}\nabla\cdot\boldsymbol{D}\boldsymbol{u}_k + \nabla p_k - A(\theta_{k-1})\boldsymbol{u}_k \\
\qquad - A'(\theta_{k-1})\theta_k\boldsymbol{u}_{k-1} - \theta_k f_B'(\theta_{k-1})\boldsymbol{e}_d = (f_B(\theta_{k-1}) - \theta_{k-1}f_B'(\theta_{k-1}))\boldsymbol{e}_d \\
\qquad\qquad - \left(\dfrac{-4\boldsymbol{u}^n + \boldsymbol{u}^{n-1}}{2\Delta t}\right) + \boldsymbol{u}_{k-1}\cdot\nabla\boldsymbol{u}_{k-1} - A'(\theta_{k-1})\theta_{k-1}\boldsymbol{u}_{k-1} \\
\nabla\cdot\boldsymbol{u}_k = 0 \\
C(\theta_{k-1})\dfrac{3}{2\Delta t}\theta_k + C'(\theta_{k-1})\left(\dfrac{3\theta_{k-1} - 4\theta^n + \theta^{n-1}}{2\Delta t}\right)\theta_k + C(\theta_{k-1})\boldsymbol{u}_k\cdot\nabla\theta_{k-1} + C(\theta_{k-1})\boldsymbol{u}_{k-1}\cdot\nabla\theta_k \\
\qquad + C'(\theta_{k-1})\boldsymbol{u}_{k-1}\cdot\nabla\theta_{k-1}\theta_k + \dfrac{3}{2\Delta t}\theta_k S'(\theta_{k-1}) - \nabla\cdot\left(K(\theta_{k-1})\nabla\theta_k + \theta_k K'(\theta_{k-1})\nabla\theta_{k-1}\right) \\
\qquad = C'(\theta_{k-1})\left(\dfrac{3\theta_{k-1} - 4\theta^n + \theta^{n-1}}{2\Delta t}\right)\theta_{k-1} - C(\theta_{k-1})\left(\dfrac{-4\theta^n + \theta^{n-1}}{2\Delta t}\right) \\
\qquad\quad + C(\theta_{k-1})\boldsymbol{u}_{k-1}\cdot\nabla\theta_{k-1} + C'(\theta_{k-1})\boldsymbol{u}_{k-1}\cdot\nabla\theta_{k-1}\theta_{k-1} \\
\qquad\quad + \dfrac{3}{2\Delta t}\theta_{k-1}S'(\theta_{k-1}) - \left(\dfrac{3S(\theta_{k-1}) - 4S(\theta^n) + S(\theta^{n-1})}{2\Delta t}\right) - \nabla\cdot\left(\theta_{k-1}K'(\theta_{k-1})\nabla\theta_{k-1}\right) \\
\boldsymbol{u}_k|_{\partial\Omega} = 0 \qquad \theta_k|_{\Gamma_{hot}} = \theta_{hot} \qquad \theta_k|_{\Gamma_{cold}} = \theta_{cold} \qquad \partial_{\boldsymbol{n}}\theta_k|_{\Gamma_a} = h_a.
\end{cases}
\tag{8}
$$

Where, using the smoothness of A, C, S, K and the differentiability of f_B (recall that we are assuming a Boussinesq approximation)

$$
A'(\theta) = \frac{d}{d\theta}A(\theta), \quad C'(\theta) = \frac{d}{d\theta}C(\theta), \quad S'(\theta) = \frac{d}{d\theta}S(\theta), \quad K'(\theta) = \frac{d}{d\theta}K(\theta), \quad f_B'(\theta) = \frac{d}{d\theta}f_B(\theta).
$$

Note that the first time step ($n = 1$) is obtained by using a simple backward Euler or Crank-Nicolson scheme, producing minor modifications in (8) for the first time step. Obviously through modification of this relatively generic algorithm we could recuperate various strategies.

3.2. Mixed decoupled scheme

As a final observation concerning the mixed approach, we present a second strategy, based on (8), targeting a decrease in computational time. It relies on decoupling the Navier–Stokes and heat equations producing two subsystems of smaller size then the original single one. Of course the number of fixed point loop is tripled as we need to solve both subsystems which are nonlinear and then recuperate the coupling through a global loop. However, as the subsystems are of smaller size it is expected that in some cases the overall computational time could be smaller. This is the starting point of the method proposed in [3]. For that strategy, introducing the combined index (k, i) for the i–th iteration of the subsystem and k–th global iteration and at each time step t^{n+1} we apply the following *mixed-decoupled algorithm*

1. *Initialization:*

$$
\boldsymbol{u}_0 = \boldsymbol{u}^n, \quad p_0 = p^n, \quad \theta_0 = \theta^n, \qquad \text{in } \Omega.
$$

2. *Determine* $(\boldsymbol{u}^{n+1}, p^{n+1}, \theta^{n+1})$ *with a fixed point: until convergence, compute* $(\boldsymbol{u}_k, p_k, \theta_k)$

$$
\begin{cases}
\textit{2.1 Determine } (\boldsymbol{u}_k, p_k) \textit{ with a fixed point : until convergence, compute } (\boldsymbol{u}_{k,i}, p_{k,i}) \\
\begin{cases}
\dfrac{3}{2\Delta t}\boldsymbol{u}_{k,i} + \boldsymbol{u}_{k,i-1}\cdot\nabla\boldsymbol{u}_{k,i} + \boldsymbol{u}_{k,i}\cdot\nabla\boldsymbol{u}_{k,i-1} - \dfrac{2}{Re}\nabla\cdot\boldsymbol{D}\boldsymbol{u}_{k,i} + \nabla p_{k,i} \\
\qquad - A(\theta_{k-1})\boldsymbol{u}_{k,i} = f_B(\theta_{k-1})\boldsymbol{e}_d - \left(\dfrac{-4\boldsymbol{u}^n + \boldsymbol{u}^{n-1}}{2\Delta t}\right) + \boldsymbol{u}_{k,i-1}\cdot\nabla\boldsymbol{u}_{k,i-1} \\
\nabla\cdot\boldsymbol{u}_{k,i} = 0 \\
\boldsymbol{u}_{k,i}|_{\partial\Omega} = 0.
\end{cases} \\
\textit{2.2 Determine } \theta_k \textit{ with a fixed point : until convergence, compute } \theta_{k,i} \\
\begin{cases}
C(\theta_{k,i-1})\dfrac{3}{2\Delta t}\theta_{k,i} + C'(\theta_{k,i-1})\left(\dfrac{3\theta_{k,i-1} - 4\theta^n + \theta^{n-1}}{2\Delta t}\right)\theta_{k,i} + C(\theta_{k,i-1})\boldsymbol{u}_k\cdot\nabla\theta_{k,i} \\
\qquad + C'(\theta_{k,i-1})\boldsymbol{u}_k\cdot\nabla\theta_{k,i-1}\theta_{k,i} + \dfrac{3}{2\Delta t}\theta_{k,i}S'(\theta_{k,i-1}) \\
\qquad - \nabla\cdot\left(K(\theta_{k,i-1})\nabla\theta_{k,i} + \theta_{k,i}K'(\theta_{k,i-1})\nabla\theta_{k,i-1}\right) \\
\qquad = C'(\theta_{k,i-1})\left(\dfrac{3\theta_{k,i-1} - 4\theta^n + \theta^{n-1}}{2\Delta t}\right)\theta_{k,i-1} - C(\theta_{k,i-1})\left(\dfrac{-4\theta^n + \theta^{n-1}}{2\Delta t}\right) \\
\qquad\quad + C'(\theta_{k,i-1})\boldsymbol{u}_k\cdot\nabla\theta_{k,i-1}\theta_{k,i-1} + \dfrac{3}{2\Delta t}\theta_{k,i-1}S'(\theta_{k,i-1}) \\
\qquad\quad - \left(\dfrac{3S(\theta_{k,i-1}) - 4S(\theta^n) + S(\theta^{n-1})}{2\Delta t}\right) - \nabla\cdot\left(\theta_{k,i-1}K'(\theta_{k,i-1})\nabla\theta_{k,i-1}\right) \\
\theta_k^{n+1}|_{\Gamma_{hot}} = \theta_{hot} \qquad \theta_k^{n+1}|_{\Gamma_{cold}} = \theta_{cold} \qquad \partial_{\boldsymbol{n}}\theta_k^{n+1}|_{\Gamma_a} = h_a.
\end{cases}
\end{cases}
\tag{9}
$$

Remark 4. Let us underline, that both of these algorithms, as well as the next ones, require some caution concerning the stopping criteria (see section 5.1) due to the heterogeneity of the unknowns and the presence of multiple loops. From a practical point of view one must take into account Re when fixing convergence tolerance for step 2.1 since this could lead to unrealistic computation time. More generally, the choice of the tolerance should be made taking into account the characteristic of the phenomenon as expressed by the main adimensional numbers Re, Pr, Ra etc. Once again, using a Newton loop on each subsystem seems more appropriate, but other strategies could be used. For instance, one could consider a second order extrapolation for the convective term in of the Navier–Stokes equation leading to a linear subsystem in step 2.1. Similar ideas could be considered for the thermal equation. On the same path, reducing the accuracy requirements for the inner loops could be considered as long as the accuracy of the outer loop is controlled.

3.3. Splitting algorithm

The method built here relies heavily on the nature and properties of the solution of Navier–Stokes as constructed by a projection method. Projection methods are known to have a bounded order of accuracy in H^1 norm inherent to the splitting of the viscous and incompressibility effects. The first versions of the projection method (the original approach of Chorin and Temam, and the first modification of Goda [26]) resulted in schemes with a $\mathcal{O}(\Delta t)$ H^1-error at best for the velocity for BDF1 and BDF2 time discretization. The projection method proposed in [47], the *rotational pressure correction projection*, overcame this barrier in accuracy. First we recall the rotational pressure correction projection as presented, for instance, in [29] for an incompressible Newtonian fluid.

At time t^{n+1}, assuming the temperature θ is known, the method consists in the following three steps: solving the viscous nonlinear system giving a *velocity prediction*, next is a projection step producing a *velocity/pressure correction* and finally the pressure updating step.

1. *Velocity prediction:*

$$\begin{cases} \dfrac{3\tilde{\boldsymbol{u}}^{n+1} - 4\boldsymbol{u}^n + \boldsymbol{u}^{n-1}}{2\Delta t} + \left(\tilde{\boldsymbol{u}}^{n+1}\cdot\nabla\right)\tilde{\boldsymbol{u}}^{n+1} - \dfrac{2}{Re}\nabla\cdot(\boldsymbol{D}\tilde{\boldsymbol{u}}^{n+1}) \\ \qquad\qquad + \nabla p^n - A(\theta(t^{n+1}))\tilde{\boldsymbol{u}}^{n+1} = f_B(\theta(t^{n+1}))\boldsymbol{e}_d \\ \tilde{\boldsymbol{u}}^{n+1} = 0 \qquad \text{on } \partial\Omega. \end{cases} \tag{10}$$

2. *Velocity and pressure corrector (Darcy equation):*

$$\begin{cases} \boldsymbol{u}^{n+1} + \dfrac{2\Delta t}{3}\nabla\varphi = \tilde{\boldsymbol{u}}^{n+1} \\ \nabla\cdot\boldsymbol{u}^{n+1} = 0 \\ \boldsymbol{u}^{n+1}\cdot\boldsymbol{n} = 0 \quad \text{on } \partial\Omega. \end{cases}$$

3. *Pressure update:*

$$p^{n+1} = p^n + \varphi - \frac{2}{Re}\nabla\cdot\tilde{\boldsymbol{u}}^{n+1}.$$

Remark 5. This scheme requires an initial pressure. In this paper, this initial pressure is assumed to be the atmospheric pressure P which translate in a null pressure in the adimensional setting, $p^0 = 0$.

Let $(\mathbf{u}, \mathrm{p}, \theta)$ be a solution of (3) and $\tilde{\boldsymbol{u}}^n$, $\boldsymbol{u}^n$ and p^n the approximation obtained with step 1 - 3 (using a BDF1 scheme for $n = 1$). From [29,18] we get the following error estimates

$$\max_n \|\mathbf{u}(t^n) - \boldsymbol{u}^n\|_{L^2} + \max_n \|\mathbf{u}(t^n) - \tilde{\boldsymbol{u}}^n\|_{L^2} \le C\Delta t^2$$
$$\max_n \|\mathbf{u}(t^n) - \boldsymbol{u}^n\|_{H^1} + \max_n \|\mathrm{p}(t^n) - p^n\|_{L^2} \le C\Delta t^{3/2}.$$

The H^1 accuracy for the velocity is $\mathcal{O}(\Delta t^{3/2})$. Using a BDF1 scheme for this projection method is also valid (then step 1 and 2 must be modified accordingly), it would lead, as expected, to a reduced order of accuracy.

Remark 6. The Darcy problem is a mixed system having $\boldsymbol{u}^{n+1}$ and φ as unknown. As we usually do for this method, we will avoid solving this system and fall back to the simpler Poisson problem followed by velocity and pressure update

$$\begin{cases} \Delta\varphi = \dfrac{3}{2\Delta t}\nabla\cdot\tilde{\boldsymbol{u}}^{n+1} \\ \partial_n\varphi = 0 \quad \text{on } \partial\Omega \end{cases}, \qquad \begin{cases} \boldsymbol{u}^{n+1} = \tilde{\boldsymbol{u}}^{n+1} - \dfrac{2\Delta t}{3\rho}\nabla\varphi \\ p^{n+1} = p^n + \varphi - \dfrac{2}{Re}\nabla\cdot\tilde{\boldsymbol{u}}^{n+1}. \end{cases} \tag{11}$$

Note that both systems (Poisson and Darcy) are ill-posed and we seek a solution in $H^1(\Omega)\backslash\mathbb{R}$ for φ.

The projection method decouple the incompressibility constraint from the diffusion operator in the momentum equation. At each time step, a velocity prediction $\tilde{\boldsymbol{u}}$ is computed from a viscous equation. Then a correction of the pressure and velocity is computed and applied. Based on the accuracy of the velocity predictor, following the idea in [16], we can introduce a decoupling of the velocity and temperature.

3.3.1. A basic mixed coupled projection (BPS) scheme

Obviously the projection approaches can be applied in system (7), giving alternatives to the standard $(\boldsymbol{u}, p)$ saddle-point formulation in (8) and (9) by replacing the mixed Navier–Stokes equation by (10)–(11). However apart from avoiding the velocity-pressure saddle-point such a direct substitution would hardly show any improvement in efficiency.

As demonstrated in [29], the L^2–error of the predicted velocity $\tilde{\boldsymbol{u}}$ has the same order of accuracy as the L^2–error of $\boldsymbol{u}^{n+1}$. As in [16] we propose an approach relying on this property of the velocity prediction: the predictor $\tilde{\boldsymbol{u}}$ can be used instead of $\boldsymbol{u}^{n+1}$ to approximate the temperature.

The first algorithm based on this idea, let us call it the *mixed coupled projection scheme*, is obtained by revisiting the mixed-coupled algorithm characterized by (8). We rewrite (8) using the velocity prediction $\tilde{\boldsymbol{u}}$ coupled to θ instead of $\boldsymbol{u}$. As the pressure and velocity are not used to solve the $(\tilde{\boldsymbol{u}}, \theta)$ system, the velocity and pressure computation (i.e. the Poisson problem and velocity-pressure update (11)) are made outside of the non-linear loop. Considering the simplification of the nonlinear loop going from (8) to (12) an obvious gain in computational efficiency is expected at this level which translate, in most case, in a gain in global efficiency of the algorithm when compared to the mixed-coupled algorithm.

1. *Initialization:*

$$\boldsymbol{u}_0 = \boldsymbol{u}^n, \quad p_0 = p^n, \quad \theta_0 = \theta^n.$$

2. *Determine $(\tilde{\boldsymbol{u}}^{n+1}, \theta^{n+1})$ as the limit of the fixed point: until convergence, compute $(\tilde{\boldsymbol{u}}_k, \theta_k)$ solution of*

$$\begin{cases} \dfrac{3}{2\Delta t}\tilde{\boldsymbol{u}}_k + \tilde{\boldsymbol{u}}_{k-1}\cdot\nabla\tilde{\boldsymbol{u}}_k + \tilde{\boldsymbol{u}}_k\cdot\nabla\tilde{\boldsymbol{u}}_{k-1} - \dfrac{2}{Re}\nabla\cdot\boldsymbol{D}\tilde{\boldsymbol{u}}_k - A(\theta_{k-1})\tilde{\boldsymbol{u}}_k \\ \quad - A'(\theta_{k-1})\theta_k\tilde{\boldsymbol{u}}_{k-1} - \theta_k f_B'(\theta_{k-1}) = (f_B(\theta_{k-1}) - \theta_{k-1}f_B'(\theta_{k-1}))\boldsymbol{e}_d - \nabla p^n \\ \quad - \left(\dfrac{-4\boldsymbol{u}^n + \boldsymbol{u}^{n-1}}{2\Delta t}\right) + \tilde{\boldsymbol{u}}_{k-1}\cdot\nabla\tilde{\boldsymbol{u}}_{k-1} - A'(\theta_{k-1})\theta_{k-1}\tilde{\boldsymbol{u}}_{k-1} \\ C(\theta_{k-1})\dfrac{3}{2\Delta t}\theta_k + C'(\theta_{k-1})\left(\dfrac{3\theta_{k-1} - 4\theta^n + \theta^{n-1}}{2\Delta t}\right)\theta_k + C(\theta_{k-1})\tilde{\boldsymbol{u}}_k\cdot\nabla\theta_{k-1} + C(\theta_{k-1})\tilde{\boldsymbol{u}}_{k-1}\cdot\nabla\theta_k \\ \quad + C'(\theta_{k-1})\tilde{\boldsymbol{u}}_{k-1}\cdot\nabla\theta_{k-1}\theta_k + \dfrac{3}{2\Delta t}\theta_k S'(\theta_{k-1}) - \nabla\cdot\left(K(\theta_{k-1})\nabla\theta_k + \theta_k K'(\theta_{k-1})\nabla\theta_{k-1}\right) \\ \qquad = C'(\theta_{k-1})\left(\dfrac{3\theta_{k-1} - 4\theta^n + \theta^{n-1}}{2\Delta t}\right)\theta_{k-1} - C(\theta_{k-1})\left(\dfrac{-4\theta^n + \theta^{n-1}}{2\Delta t}\right) \\ \qquad\quad + C(\theta_{k-1})\tilde{\boldsymbol{u}}_{k-1}\cdot\nabla\theta_{k-1} + C'(\theta_{k-1})\tilde{\boldsymbol{u}}_{k-1}\cdot\nabla\theta_{k-1}\theta_{k-1} + \dfrac{3}{2\Delta t}\theta_{k-1}S'(\theta_{k-1}) \\ \qquad\quad - \left(\dfrac{3S(\theta_{k-1}) - 4S(\theta^n) + S(\theta^{n-1})}{2\Delta t}\right) - \nabla\cdot\left(\theta_{k-1}K'(\theta_{k-1})\nabla\theta_{k-1}\right) \\ \boldsymbol{u}_k|_{\partial\Omega} = 0 \qquad \theta_k|_{\Gamma_{hot}} = \theta_{hot} \qquad \theta_k|_{\Gamma_{cold}} = \theta_{cold} \qquad \partial_{\boldsymbol{n}}\theta_k|_{\Gamma_a} = h_a. \end{cases} \tag{12}$$

3. *Projection step:compute φ solution of the Poisson problem*

$$\Delta\varphi = \frac{3}{2\Delta t}\nabla\cdot\tilde{\boldsymbol{u}}^{n+1} \qquad \partial_n\varphi = 0 \quad \text{on } \partial\Omega.$$

4. *Velocity and pressure correction:*

$$\boldsymbol{u}^{n+1} = \tilde{\boldsymbol{u}}^{n+1} - \frac{2\Delta t}{3\rho}\nabla\varphi, \quad p^{n+1} = p^n + \varphi - \frac{2}{Re}\nabla\cdot\tilde{\boldsymbol{u}}^{n+1}. \tag{13}$$

3.3.2. A coupled projection (CPS) scheme

Finally we can break (12) in smaller and simpler steps and introduce two subsystems. Once again the price for these smaller systems is the necessity to have more fixed point loops. The observations in Remark 4 are still valid: simpler subsystems could be considered or reduced accuracy requirements for the inner-loop, however, from our numerical experience, reducing the accuracy of the outer-loop should be avoided.

Decoupling the $(\tilde{\boldsymbol{u}}, \theta)$ system (12) produce an algorithm that we will call a *coupled projection scheme* since it is a extension of the CPS proposed in [16]. It corresponds to the use of the prediction velocity instead of $\boldsymbol{u}^{n+1}$ in the mixed decoupled algorithm characterized by (9). At each time step, we have the following procedure:

1. *Initialization:*

$$\tilde{\boldsymbol{u}}_0 = \boldsymbol{u}^n, \quad \theta_0 = \theta^n \qquad \text{in } \Omega.$$

2. *Determine $(\tilde{\boldsymbol{u}}^{n+1}, \theta^{n+1})$ with a fixed point: until convergence, compute $(\tilde{\boldsymbol{u}}_k, \theta_k)$*

$$
\begin{cases}
\textit{2.1 Determine } \tilde{\boldsymbol{u}}_k \textit{ with a fixed point : until convergence, compute } \tilde{\boldsymbol{u}}_{k,i} \\
\begin{cases}
\dfrac{3}{2\Delta t}\tilde{\boldsymbol{u}}_{k,i} + \tilde{\boldsymbol{u}}_{k,i-1}\cdot\nabla\tilde{\boldsymbol{u}}_{k,i} + \tilde{\boldsymbol{u}}_{k,i}\cdot\nabla\tilde{\boldsymbol{u}}_{k,i-1} - \dfrac{2}{Re}\nabla\cdot\boldsymbol{D}\tilde{\boldsymbol{u}}_{k,i} - A(\theta_{k-1})\tilde{\boldsymbol{u}}_{k,i} \\
\qquad = f_B(\theta_{k-1})\boldsymbol{e}_d - \nabla p^n - \left(\dfrac{-4\boldsymbol{u}^n + \boldsymbol{u}^{n-1}}{2\Delta t}\right) + \tilde{\boldsymbol{u}}_{k,i-1}\cdot\nabla\tilde{\boldsymbol{u}}_{k,i-1} \\
\tilde{\boldsymbol{u}}_{k,i}|_{\partial\Omega} = 0.
\end{cases} \\
\textit{2.2 Determine } \theta_k \textit{ with a fixed point : until convergence, compute } \theta_{k,i} \\
\begin{cases}
C(\theta_{k,i-1})\dfrac{3}{2\Delta t}\theta_{k,i} + C'(\theta_{k,i-1})\left(\dfrac{3\theta_{k,i-1} - 4\theta^n + \theta^{n-1}}{2\Delta t}\right)\theta_{k,i} + C(\theta_{k,i-1})\tilde{\boldsymbol{u}}_k\cdot\nabla\theta_{k,i} \\
\quad + C'(\theta_{k,i-1})\tilde{\boldsymbol{u}}_k\cdot\nabla\theta_{k,i-1}\theta_{k,i} + \dfrac{3}{2\Delta t}\theta_{k,i}S'(\theta_{k,i-1}) \\
\quad - \nabla\cdot\left(K(\theta_{k,i-1})\nabla\theta_{k,i} + \theta_{k,i}K'(\theta_{k,i-1})\nabla\theta_{k,i-1}\right) \\
\quad = C'(\theta_{k,i-1})\left(\dfrac{3\theta_{k,i-1} - 4\theta^n + \theta^{n-1}}{2\Delta t}\right)\theta_{k,i-1} - C(\theta_{k,i-1})\left(\dfrac{-4\theta^n + \theta^{n-1}}{2\Delta t}\right) \\
\qquad + C'(\theta_{k,i-1})\tilde{\boldsymbol{u}}_k\cdot\nabla\theta_{k,i-1}\theta_{k,i-1} + \dfrac{3}{2\Delta t}\theta_{k,i-1}S'(\theta_{k,i-1}) \\
\qquad - \left(\dfrac{3S(\theta_{k,i-1}) - 4S(\theta^n) + S(\theta^{n-1})}{2\Delta t}\right) - \nabla\cdot\left(\theta_{k,i-1}K'(\theta_{k,i-1})\nabla\theta_{k,i-1}\right) \\
\theta_k^{n+1}|_{\Gamma_{hot}} = \theta_{hot} \qquad \theta_k^{n+1}|_{\Gamma_{cold}} = \theta_{cold} \qquad \partial_{\boldsymbol{n}}\theta_k^{n+1}|_{\Gamma_a} = h_a.
\end{cases}
\end{cases}
\tag{14}
$$

3. *Projection step:compute φ solution of the Poisson problem*

$$\Delta\varphi = \frac{3}{2\Delta t}\nabla\cdot\tilde{\boldsymbol{u}}^{n+1} \qquad \partial_n\varphi = 0 \quad \text{on } \partial\Omega.$$

4. *Velocity and pressure correction:*

$$\boldsymbol{u}^{n+1} = \tilde{\boldsymbol{u}}^{n+1} - \frac{2\Delta t}{3}\nabla\varphi, \quad p^{n+1} = p^n + \varphi - \frac{2}{Re}\nabla\cdot\tilde{\boldsymbol{u}}^{n+1}. \tag{15}$$

Remark 7. Considering the construction of φ (in this semi-discrete or in a totally discrete form the sum of function in (13) or (15) has to be specified since there is, a priori, no reason for these sum to be valid in a pointwise sense. The fundamental element of the projection method is the Helmoltz decomposition, see for instance [10,25] which is true in a distribution sense. Therefore the velocity and pressure decomposition in (13) and (15) must be interpreted as weak equality in the velocity and pressure space respectively.

4. Finite element discretization

Our main goal in the last two sections is to illustrate the validity of the CPS method as a suitable alternative to the mixed coupled or decoupled scheme (8) and (9). We are not aiming at performance comparison therefore will not reformulate all four schemes, but focus on the CPS discretization. Obviously numerical illustrations necessitate the full discretization of the method. Various Galerkin type methods could be used, here we chose the finite element method for the spatial discretization. For details concerning this method in the context of fluid mechanic we refer to readers to [18,33].

We introduce Ω_h a partitioning of Ω composed of triangles, quadrangles or both for $\Omega\in\mathbb{R}^2$ or tetrahedra, hexahedra or both for $\Omega\in\mathbb{R}^3$. At each time step t^{n+1}, we are now seeking approximations

$$\tilde{\boldsymbol{u}}_h^{n+1},\ \boldsymbol{u}_h^{n+1},\ p_h^{n+1},\ \theta_h^{n+1},\ \varphi_h.$$

Since the discrete inf–sup condition must be respected for the prediction equation (10), (12) and (14) (see [9,28] for the details and other choices) a quadratic element (P_2 interpolation) was chosen for both velocities ($\tilde{\boldsymbol{u}}_h^{n+1}$, $\boldsymbol{u}_h^{n+1}$) and a linear interpolation for the pressure. Finally, the temperature and the function φ are also quadratic. Regarding the approximation of φ, a priori, it could be of arbitrary interpolating degree, however we must take into account that φ is solution of a Poisson problem and that it act as velocity and pressure corrections.

The discrete version of Step 2 of the CPS (the fixed-point loop (14)) and Step 3 are obvious. The last step, Step 4, is splitted in two separated steps, 4_h for the velocity and 5_h for the pressure. As underlined in Remark 6, the discrete version of Step 3 must be treated in a special manner as the discrete system is under-determined. A unique solution φ_h is determined through a supplementary computation included in the last step (see Step 5_h below). Following Remark 7 to complete the spatial discretization of the algorithm a proper interpretation of Step 4 is needed. We chose to interpret both equalities as L^2–projection. Step 4_h is the L^2–projection of $\nabla\varphi_h$ in $\boldsymbol{V}_h$ a space of continuous piecewise P_2 interpolation. Step 5_h is the projection of $\nabla\cdot\tilde{\boldsymbol{u}}$ and φ_h in a space of continuous piecewise P_1 approximation noted M_h.

4_h. *Velocity correction:* Compute $\boldsymbol{u}_h^{n+1}\in\boldsymbol{V}_h$ solution of:

$$\int_{\Omega_h}\boldsymbol{u}_h^{n+1}\boldsymbol{v}\,d\Omega = \int_{\Omega_h}\tilde{\boldsymbol{u}}_h^{n+1}\cdot\boldsymbol{v}\,d\Omega - \frac{2\Delta t}{3}\int_{\Omega_h}\nabla\varphi_h\cdot\boldsymbol{v}\,d\Omega \qquad \forall\boldsymbol{v}\in\boldsymbol{V}_h.$$

5_h. *Pressure correction:* Compute $p_h^{n+1}\in M_h$ solution of

$$\int_{\Omega_h}p_h^{n+1}\zeta\,d\Omega = \int_{\Omega_h}p_h^n\zeta\,d\Omega + \int_{\Omega_h}\left(\varphi_h - \frac{2}{Re}\nabla\cdot\tilde{\boldsymbol{u}}_h^{n+1} - \mu(\varphi_h)\right)\zeta\,d\Omega \qquad \forall\zeta\in M_h$$

with

$$\mu(\varphi_h) = \frac{1}{mes(\Omega_h)} \int_{\Omega_h} \varphi_h \, d\Omega.$$

Remark 8. In Step 5_h, $\mu(\cdot)$ correspond to an average on Ω_h of φ_h. This correction gives $\varphi_h \in M_h^{\varphi} \backslash \mathbb{R}$ insuring the uniqueness of the projection in Step 5_h.

Remark 9. Following Remark 7, the projection in steps 4_h and 5_h seems to be the most natural and practical choice. Other approaches such as gradient reconstruction [51] for both steps, or the use of hierarchical interpolation for φ_h (to avoid the projection of φ_h in 5_h) are either computationally expensive or results in loss of information.

5. Numerical illustration

In this section, we test the accuracy and the capability of our proposed CPS algorithm (14) using four benchmark cases commonly used in the literature for phase-change problems with convection. First test is about natural convection of air based on a manufactured solution. This example illustrates the temporal accuracy of our proposed algorithm. Second and third cases are about water solidification and octadecane melting, respectively. In both cases, we compare our numerical solutions with the literature's experimental and numerical results. Last case consists of a challenging melting problem with a high Rayleigh number.

Our intention is not to establish the relative merit of the various methods or to study the computational performance of the CPS but to illustrate the relevance of the approach and the capability of scheme. All our numerical solutions were obtained using FreeFem++ software [32]. Computational aspects such as numerical efficiency and high performance implementation of the algorithm were not considered.

From recent works [3,4,15] mesh adaptation is clearly essential in the finite element simulation of phase change problems. Firstly, for a fixed accuracy, equidistribution of the error (one of the attributes of mesh adaptation) allows to reduce number of vertex, reducing the size of the discrete algebraic system to solve. Secondly, as the mesh is refined in the vicinity of the liquid-solid interface and the thickness of the transition zone is fixed the capture of the interface is sharper, giving a more precise definition of the interface. Thirdly, as the transition zone of fixed size is always sufficiently discretized we avoid sudden loss of convergence that are frequent when using a fixed mesh. Coherent with those observations, in all our tests, with the exception of the accuracy test, we have used mesh adaptation at each time steps. Following [15] the mesh adaptation is based on θ, $\boldsymbol{u}$ and S. As most of these problems exhibit a slow dynamic, the initial mesh size in all cases is $h = 0.01$ (all our tests are on a unit square).

5.1. Stopping criterion

Considering the great variety of scales between the unknowns involved in the different loops, it seems important to specify the strategy used to establish convergence. Let us introduce the relative errors used as stopping criteria to control the convergence: Let k be the index for the k-th iteration of the fixed-point. Based on the respective functional norm $\|\cdot\|_m$ for the velocity predictionand temperature. We introduce the relative variation,

$$err_{m_u}(\tilde{\boldsymbol{u}}_k) = \max_{1\le i\le d} \left\| \frac{(\tilde{\boldsymbol{u}}_k - \tilde{\boldsymbol{u}}_{k-1})_i}{(\tilde{\boldsymbol{u}}_{k-1})_i} \right\|_{m_u}, \quad err_{m_\theta}(\theta_k) = \left\| \frac{\theta_k - \theta_{k-1}}{\theta_{k-1}} \right\|_{m_\theta}.$$

In practice we choose $m_u = m_\theta = \infty$, corresponding to the pointwise maximal relative variation. For example, for the temperature we have

$$err_{\infty}(\theta_k) = \sup_{x\in\Omega} \frac{|\theta_k(\boldsymbol{x}) - \theta_{k-1}(\boldsymbol{x})|}{|\theta_{k-1}(\boldsymbol{x})|}.$$

Based on these definitions, the control of the convergence of the outer loop in (14) (or the loop (12)) is based on a criterion of the form

$$\max\left\{ err_{m_u}(\tilde{\boldsymbol{u}}_k), err_{m_\theta}(\theta_k) \right\} < \text{Tol},$$

where Tol is a small tolerance. Since all these variations are relative, using a single tolerance for all variables should suffice. As for the inner loop in (14) we use the corresponding relative criteria. For the mixed (coupled or decoupled) algorithms, a pressure tolerance would be added for (8), the outer loop of (9) and the Navier-Stokes loop inside (9).

Remark 10. The usual trade off between computational costs and precision must be considered. Concerning the flow variable, one must take into account the important impact of the Reynold number Re which can lead to unrealistic computation time for certain tolerance. The choice of the tolerance for both inner loops in (9) and (14) should be made taking into account the characteristic of the phenomenon as expressed by the main adimensional numbers Re, Pr, Ra etc.

5.2. Accuracy test with a manufactured solution

In this example, we test the time accuracy of our numerical method using a manufactured solution on a square $[0,1]\times[0,1]$. We consider $C = k = 1$, we set $A(\theta) = S(\theta) = 0$ and fixed $Re = 1$, $Pr = 10$, and $Ra = 10^3$ or $Ra = 10^6$.

$$\begin{cases} u_1(x,y,t) = (x^2 + 2xy + 3y - 4)\sin(t), \\ u_2(x,y,t) = (-y^2 - 2xy + x^2 - 2x + 3)\sin(t) + t^3, \\ T(x,y,t) = (x^2 - 2y^2 - 4xy + 2)e^t, \\ p(x,y,t) = (x - y)\sin(t). \end{cases}$$

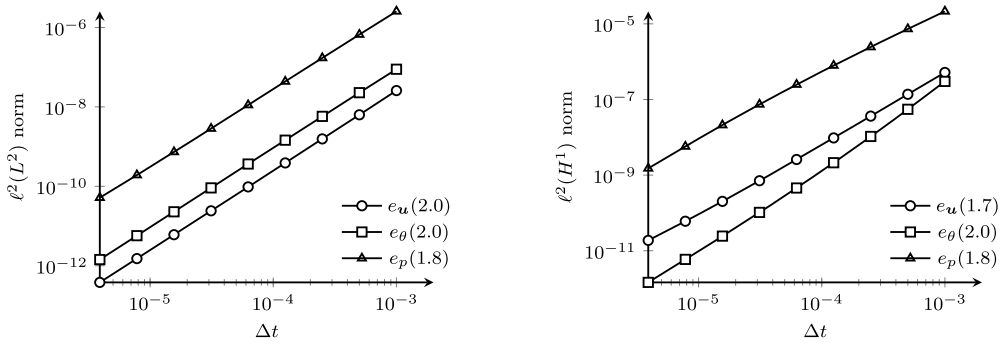

Fig. 1. Accuracy test, $Re = 1$, $Pr = 10$ and $Ra = 1e3$. ℓ^2 norm between the analytical and numerical solutions using the coupled projection scheme. In parentheses the computed order of accuracy.

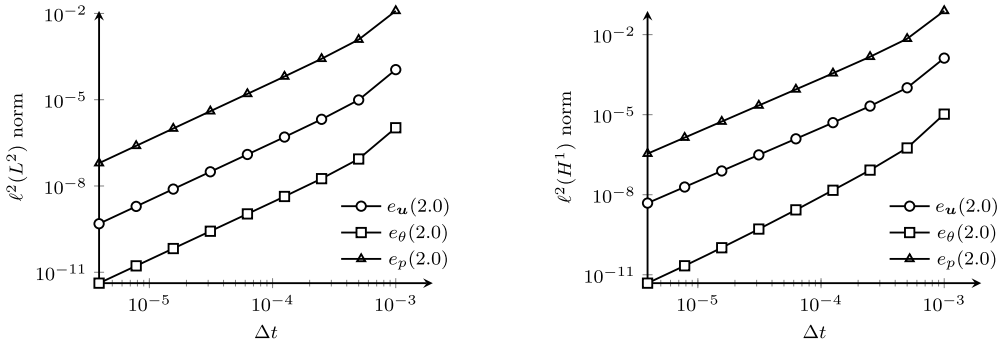

Fig. 2. Accuracy test, $Re = 1$, $Pr = 10$ and $Ra = 1e6$. ℓ^2 norm between the analytical and numerical solutions using the coupled projection scheme. In parentheses the computed order of accuracy.

The velocity, pressure and temperature error to the exact solution will be computed using a ℓ^2 norm. Denoted $e_{\boldsymbol{u}}$, e_p and e_θ they are defined as follows:

$$\|e_Q\|_{\ell^2(S)} = \left(\Delta t \sum_n \|Q(t^n) - Q^n\|_S^2 \right)^{1/2}$$

with $Q \in \{\boldsymbol{u}, p, \theta\}$, $S = L^2(\Omega)$ or $\boldsymbol{L}^2(\Omega) = \left(L^2(\Omega)\right)^d$ and $S = H^1(\Omega)$ or $\boldsymbol{H}^1(\Omega) = \left(H^1(\Omega)\right)^d$. We consider a regular mesh using a 40×40 uniform grid a series of time step length $\Delta t = 0.001/2^p$ for p between 0 and 8. The errors are computed for a final time $t_{max} = 0.01$.

The results are presented in Figs. 1 and 2. As can be seen, a variation of three order in the Rayleigh number as little impact on the order of accuracy. We obtained the expected second order convergence for the velocity, pressure and temperature (see left of Fig. 1 and 2). Using the $\ell^2(H^1)$, a second order of convergence was obtained for the temperature, while the convergence order for the velocity and pressure were approximately 2 for both values of Ra (see right of Fig. 1 and 2). This is in agreement with the results of convergence of projection schemes (see for example [29]) where the convergence rate is reported to be at least $3/2$.

5.3. Water solidification

Freezing of water is a very common phase change problem. In the experimental results, the ice front is almost perpendicular to the bottom wall (see [34,35]). In many numerical results ([23,24,34]), important discrepancies in the ice front form were noticed. However, the recent numerical results ([40,3,15,6,7]) have shown a good agreement between numerical and experimental results. In this section, we validate the effectiveness of the proposed projection scheme to this type of solidification problem. Our numerical simulations (denoted CPS schemes in the various figures) are compared to the experimental results in [34] and numerical results in [3] and [40]. In this example, temperature differences in the melted region give rise to nonlinear buoyancy forces that produce significant convective flow. This flow induces modifications in the heat transfer and the position of the interface. We employ the variable density suggested in [22]:

$$\rho(T) = \rho_m(1 - w(T - T_m)^q)$$

with $\rho_m = 999.972$ [kg/m^3], $w = 9.2793.10^{-6}$ ([^{o}C])$^{-q}$ and $q = 1.894816$. The buoyancy force in this case can be written as

$$f_B(\theta) = \frac{Ra}{PrRe^2} \frac{1}{\beta \delta T} \frac{\rho(\theta_{cold}) - \rho(\theta)}{\rho(\theta_{cold})},$$

where $\beta = \rho/(\Delta t \rho_m)$ is the thermal expansion coefficient with $\beta = 6.91 \times 10^{-5}$ [K^{-1}]. The dimensional parameters of the problem are $Re = 1$, $Pr = 6.99$, $Ra = 2.518084 \times 10^6$ and $Ste = 0.125$. For the initial condition of this simulation, velocity and pressure are null and the initial fluid temperature is just above the freezing point (a "cold start"). The mesh size h equal to $= 0.01$, a time step $\Delta t = 10^{-3}$ and the width of the mushy zone $\varepsilon = 0.03$. The Carman–Kozeny constant $C_A = 10^6$ and the penalty parameter $b = 10^{-6}$.

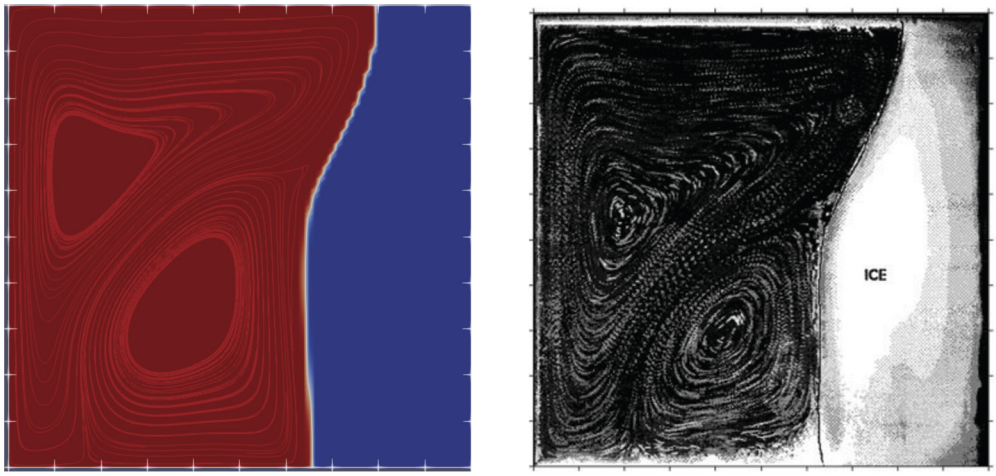

Fig. 3. Water Freezing at $t = 2340s$. On the left: Projection method; On the right: Experiment of Kowalewski [34].

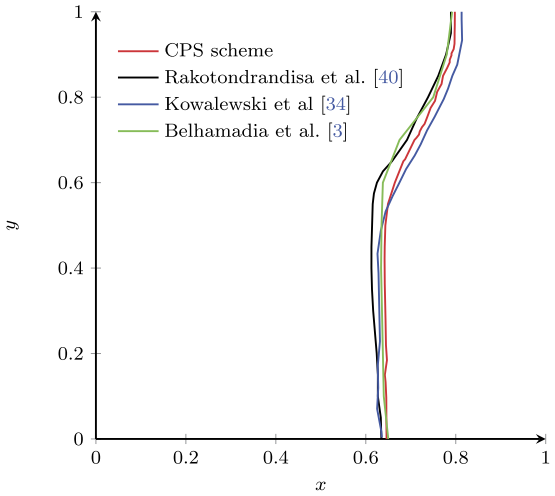

Fig. 4. Water solidification: Comparison of the solid-liquid interface at $t = 2340$ s.

A comparison between our numerical solution and the experimental result performed in [34] is presented in Fig. 3. As can be seen, we obtain a good agreement between numerical and experimental results for water freezing. Good agreement between numerical and experimental results has also been obtained in [3] and [40]. In [3] a mixed formulation for Navier–Stokes equations coupled with a mixed formulation for the energy equations has been employed and in [40] a coupled mixed formulation has been used. Fig. 4 shows the solid-liquid interface position for water solidification presented in these contributions compared to interface position obtained with our coupled projection scheme. As illustrated in this figure, all results are very similar.

5.4. Melting of octadecane in a square cavity

In this test case, we consider the melting of octadecane in a square cavity. This benchmark is often used to validate numerical simulations for phase change problems (see [15], [40] and [50]) in comparison with experimental results performed in [37]. In [15] a first order in time coupled mixed formulation has been used and in [40] a second order in time coupled mixed formulation has been employed for the numerical simulations. In [50], the numerical results were obtained with a consistent update technique (CUT) algorithm, where the velocity and pressure satisfy the momentum equations explicitly and the continuity equation implicitly (the results were compared to numerical solutions obtained by a SIMPLE algorithm that is widely used to solve pressure-linked Navier–Stokes equations).

In this test, a solid cavity filled by octadecane is heated from the left wall by imposing a Dirichlet boundary condition $\theta_{hot} = 1$ and a fixed (cold) temperature is imposed on the right side $\theta_{cold} = -0.01$. Top and bottom boundaries are adiabatic. The dimensionless parameters are the Prandtl number $Pr = 56.2$, the Rayleigh number $Ra = 3.27e5$ and the Stefan number $Ste = 0.045$. As for the numerical parameters used for this simulation: the size of the mesh is fixed at $h = 0.01$, the time step $\Delta t = 10^{-3}$ and the width of the mushy zone $\varepsilon = 0.03$.

In Fig. 5 we compare the evolution of the solid-liquid interface at time $t = 39.9$ s and $t = 78.7$ s with the experimental and numerical data in [37] and the numerical results obtained in [50,15,40]. We notice that the shape and position of the liquid-solid interface is in agreement with the experimental results in [37] and similar to the recent work performed in [40].

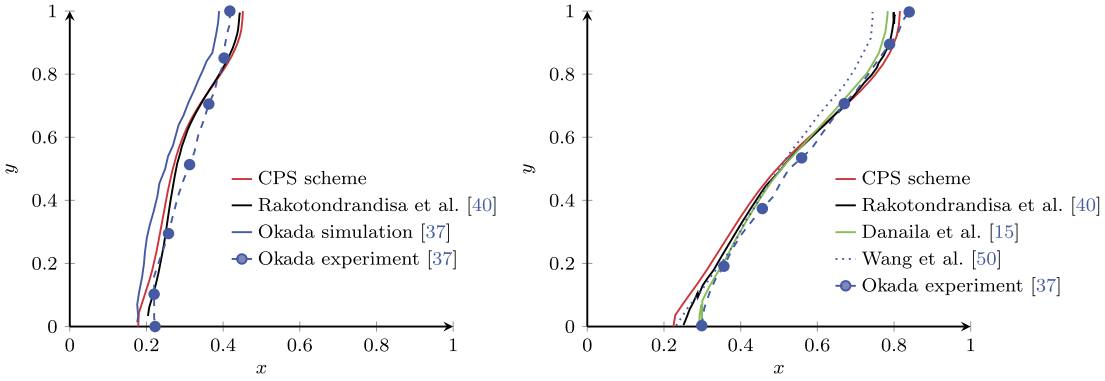

Fig. 5. Melting of Octadecane $Ra = 3.27 \times 10^5$. On the left, position of the interface at time $t = 39.9$ s. On the right position of the interface at time $t = 78.8$ s.

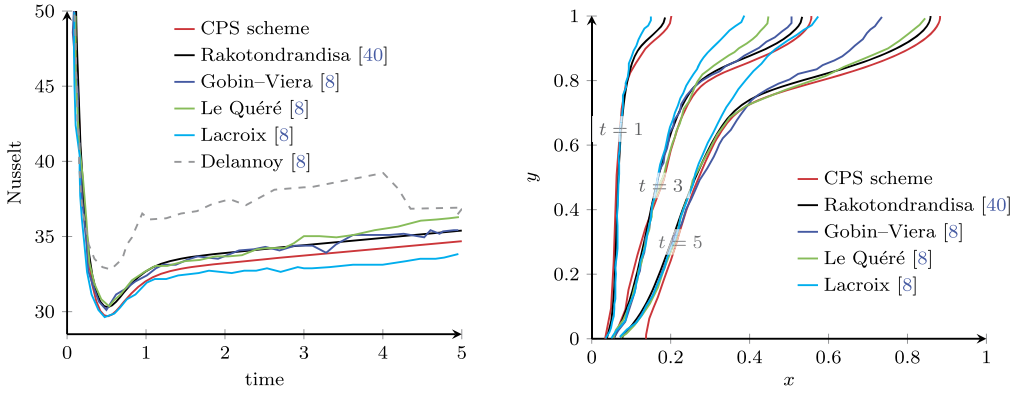

Fig. 6. Melting of Octadecane with $Ra = 10^8$: on the left, time evolution of the Nusselt number. On the right position of the interface at time $t = 1$, $t = 3$, and $t = 5$.

5.5. Melting of octadecane with high Rayleigh number

In this case, we consider the same melting problem as in the previous test, but with a very high value of the Rayleigh number. This test is frequently treated in the literature and is known as a very challenging case as the natural convection becomes important in the fluid flow. For this test, the following dimensionless parameters are imposed: the Prandtl number $Pr = 50$, the Rayleigh number $Ra = 10^8$ and the Stefan number $Ste = 0.1$. The simulations were done with a mesh size of $h = 0.01$, a time step $\Delta t = 10^{-4}$ and width of the mushy zone $\epsilon = 0.03$.

In [8] a first collection of results, by different authors, concerning this and other benchmark is presented. More recently, [40] proposed some numerical results for this test using a second order in time coupled mixed formulation. As observed in [8], such a high Rayleigh number is numerically very demanding and can lead to unrealistic numerical results (see Fig. 6 on the left, the results of Delannoy).

We qualitatively compared our results to various results presented in [8] in terms of Nusselt number time evolution and position of the solid-liquid interface at times $t = 1$ s, $t = 3$ s, and $t = 5$ s. This comparison is presented in Figs. 6 (left for the Nusselt number and right for the interface position at different time value). From Fig. 6 the results obtained for the shape and position of the liquid-solid interface and for the Nusselt evolution with our method are in good agreement with those presented in [8] and [40].

6. Conclusion

We proposed a projection method for the numerical simulation of phase change problems with natural convection for the melting-solidification of solid-liquid phases. We illustrated the convergence of the algorithm by a manufactured solution. We proved the effectiveness of the algorithm by comparing to real experiment of the water solidification and melting of octadecane even with high Rayleigh number. The following step is to compare rigorously the computational cost of the proposed projection scheme and the mixed formulation for both melting and solidification problems. It will also be interesting to extend previous work [3] to investigate the efficiency of the parallel anisotropic mesh adaptation technique [1] on the three-dimensional phase change problem with convection. This topic will be subject of a future work.

Acknowledgements

The second author gratefully acknowledges the financial support of the American University of Sharjah Enhanced Faculty Research Grant. The work in this paper was supported, in part, by the Open Access Program from the American University of Sharjah. This paper represents the opinions of the author(s) and does not mean to represent the position or opinions of the American University of Sharjah.

References

[1] Y. Belhamadia, T. Briffard, A. Fortin, Application of parallel anisotropic mesh adaptation for solving monodomain cardiac model, AIP Conference Proceedings 2343 (2021).
[2] Y. Belhamadia, A time-dependent adaptive remeshing for electrical waves of the heart, IEEE Trans. Biomed. Eng. 55 (2, Part-1) (2008) 443–452.

[3] Y. Belhamadia, A. Fortin, T. Briffard, Two-dimensional adaptive remeshing method for solving melting and solidification phase change problems with convection, Numer. Heat Transf., Part A, Appl. 76 (4) (2019) 179–197.
[4] Y. Belhamadia, A. Fortin, É. Chamberland, Anisotropic mesh adaptation for the solution of the Stefan problem, J. Comput. Phys. 194 (1) (2004) 233–255.
[5] Y. Belhamadia, A. Fortin, É. Chamberland, Three-dimensional anisotropic mesh adaptation for phase change problems, J. Comput. Phys. 201 (2) (2004) 753–770.
[6] Y. Belhamadia, A.S. Kane, A. Fortin, An enhanced mathematical model for phase change problems with natural convection, Int. J. Numer. Anal. Model. Ser. B 3 (2) (2012) 192–206.
[7] Y. Belhamadia, A.S. Kane, A. Fortin, A mixed finite element formulation for solving phase change problems with convection, in: Proceedings of the 20th Annual Conference of the CFD Society of Canada, 2012.
[8] O. Bertrand, B. Binet, H. Combeau, S. Couturier, Y. Delannoy, D. Gobin, M. Lacroix, P. Le Quéré, M. Médale, J. Mencinger, S. Hamou, G. Vieira, Melting driven by natural convection a comparison exercise: first results, Int. J. Therm. Sci. 38 (1) (1999) 5–26.
[9] D. Boffi, F. Brezzi, M. Fortin, Mixed Finite Element Methods and Applications, Springer Series in Computational Mathematics, vol. 44, Springer Berlin Heidelberg, Berlin, Heidelberg, 2013.
[10] F. Boyer, P. Fabrie, Mathematical Tools for the Study of the Incompressible Navier-Stokes Equations and Related Models, Applied Mathematical Sciences, vol. 183, Springer, New York, 2013.
[11] A.D. Brent, V.R. Voller, K.J. Reid, Enthalpy-porosity technique for modeling convection-diffusion phase change: application to the melting of a pure metal, Numer. Heat Transf. 13 (3) (April 1988) 297–318.
[12] Y. Cao, A. Faghri, W.S. Chang, A numerical analysis of Stefan problems for generalized multi-dimensional phase-change structures using the enthalpy transforming model, Int. J. Heat Mass Transf. 32 (7) (July 1989) 1289–1298.
[13] A.J. Chorin, Numerical solution of the Navier–Stokes equations, Math. Comput. 22 (1968) 745–762.
[14] A.J. Chorin, On the convergence of discrete approximations to the Navier–Stokes equations, Math. Comput. 23 (1969) 341–353.
[15] I. Danaila, R. Moglan, F. Hecht, S. Le Masson, A Newton method with adaptive finite elements for solving phase-change problems with natural convection, J. Comput. Phys. 274 (October 2014) 826–840.
[16] J. Deteix, A. Jendoubi, D. Yakoubi, A coupled prediction scheme for solving the Navier–Stokes and convection-diffusion equations, SIAM J. Numer. Anal. 52 (5) (2014) 2415–2439.
[17] J. Deteix, D. Yakoubi, Improving the pressure accuracy in a projection scheme for incompressible fluids with variable viscosity, Appl. Math. Lett. 79 (2018) 111–117.
[18] Alexandre Ern, Jean-Luc Guermond, Theory and Practice of Finite Elements, Applied Mathematical Sciences, vol. 159, Springer, New York, NY, 2004.
[19] K.J. Evans, D.A. Knoll, Temporal accuracy analysis of phase change convection simulations using the JFNK-SIMPLE algorithm, Int. J. Numer. Methods Fluids 55 (7) (2007) 637–653.
[20] K.J. Evans, D.A. Knoll, M. Pernice, Development of a 2-D algorithm to simulate convection and phase transition efficiently, J. Comput. Phys. 219 (1) (November 2006) 404–417.
[21] W.F. Florez, H. Power, F. Chejne, Numerical solution of thermal convection problems using the multidomain boundary element method, Numer. Methods Partial Differ. Equ. 18 (4) (2002) 469–489.
[22] B. Gebhart, J.C. Mollendorf, A new density relation for pure and saline water, Deep-Sea Res. 24 (9) (September 1977) 831–848.
[23] M. Giangi, T.A. Kowalewski, F. Stella, E. Leonardi, Natural convection during ice formation: numerical simulation vs. experimental results, Comput. Assist. Mech. Eng. Sci. 7 (3) (2000) 321–342.
[24] M. Giangi, F. Stella, T.A. Kowalewski, Phase change problems with free convection: fixed grid numerical simulation, Comput. Vis. Sci. 2 (1999) 123–130.
[25] V. Girault, P.-A. Raviart, Finite Element Methods for the Navier-Stokes Equations, Springer Series in Computational Mathematics, vol. 5, Springer-Verlag, Berlin, 1986.
[26] K. Goda, A multistep technique with implicit difference schemes for calculating two- or three-dimensional cavity flows, J. Comput. Phys. 30 (1) (1979) 76–95.
[27] P.M. Gresho, R.L. Lee, S.T. Chan, R.L. Sani, Solution of the time-dependent incompressible Navier-Stokes and Boussinesq equations using the Galerkin finite element method, in: Reimund Rautmann (Ed.), Approximation Methods for Navier-Stokes Problems, Springer Berlin Heidelberg, Berlin, Heidelberg, 1980, pp. 203–222.
[28] J.L. Guermond, P. Minev, J. Shen, Error analysis of pressure-correction schemes for the time-dependent Stokes equations with open boundary conditions, SIAM J. Numer. Anal. 43 (1) (2006) 239–258.
[29] J.L. Guermond, P. Minev, Jie Shen, An overview of projection methods for incompressible flows, Comput. Methods Appl. Mech. Eng. 195 (44–47) (September 2006) 6011–6045.
[30] S.C. Gupta, A moving grid numerical scheme for multi-dimensional solidification with transition temperature range, Comput. Methods Appl. Mech. Eng. 189 (2) (2000) 525–544.
[31] N. Hannoun, V. Alexiades, T.Z. Mai, Resolving the controversy over tin and gallium melting in a rectangular cavity heated from the side, Numer. Heat Transf., Part B, Fundam. 44 (3) (September 2003) 253–276.
[32] F. Hecht, New development in FreeFem ++ , J. Numer. Math. 20 (3–4) (2012) 251–265.
[33] Volker John, Finite Element Methods for Incompressible Flow Problems, Springer, 2016.
[34] T.A. Kowalewski, M. Rebow, Freezing of water in a differentially heated cubic cavity, Int. J. Comput. Fluid Dyn. 11 (3–4) (January 1999) 193–210.
[35] T.A. Kowalewski, M. Rebow, An experimental benchmark for freezing water in the cubic cavity, in: Adv. in Computational Heat Transfer, 1998, pp. 149–156.
[36] P. Nithiarasu, A unified fractional step method for compressible and incompressible flows, heat transfer and incompressible solid mechanics, Int. J. Numer. Methods Heat Fluid Flow 18 (2) (2008) 111–130.
[37] M. Okada, Analysis of heat transfer during melting from a vertical wall, Int. J. Heat Mass Transf. 27 (11) (November 1984) 2057–2066.
[38] M.A. Rady, A.K. Mohanty, Natural convection during melting and solidification of pure metals in a cavity, Numer. Heat Transf., Part A, Appl. 29 (1) (1996) 49–63.
[39] A. Rakotondrandisa, I. Danaila, L. Danaila, Numerical modelling of a melting-solidification cycle of a phase-change material with complete or partial melting, Int. J. Heat Fluid Flow 76 (2019) 57–71.
[40] A. Rakotondrandisa, G. Sadaka, I. Danaila, A finite-element toolbox for the simulation of solid–liquid phase-change systems with natural convection, Comput. Phys. Commun. 253 (August 2020) 107188.
[41] F. Stella, M. Giangi, Melting of a pure metal on a vertical wall: numerical simulation, Numer. Heat Transf., Part A, Appl. 38 (2000) 193–208.
[42] K.R. Sultana, S.R. Dehghani, K. Pope, Y.S. Muzychka, Numerical techniques for solving solidification and melting phase change problems, Numer. Heat Transf., Part B, Fundam. 73 (3) (2018) 129–145.
[43] R. Temam, Une méthode d'approximation de la solution des équations de Navier–Stokes, Bull. Soc. Math. Fr. 96 (1968) 115–152.
[44] R. Temam, Sur l'approximation de la solution des équations de Navier-Stokes par la méthode des pas fractionnaires (I), Arch. Ration. Mech. Anal. 32 (2) (January 1969) 135–153.
[45] R. Temam, Sur l'approximation de la solution des équations de Navier-Stokes par la méthode des pas fractionnaires (II), Arch. Ration. Mech. Anal. 33 (5) (January 1969) 377–385.
[46] R.T. Tenchev, J.A. Mackenzie, T.J. Scanlon, M.T. Stickland, Finite element moving mesh analysis of phase change problems with natural convection, Int. J. Heat Fluid Flow 26 (4) (August 2005) 597–612.
[47] L.J.P. Timmermans, P.D. Minev, F.N. Van De Vosse, An approximate projection scheme for incompressible flow using spectral elements, Int. J. Numer. Methods Fluids 22 (7) (1996) 673–688.
[48] G. Vidalain, L. Gosselin, M. Lacroix, An enhanced thermal conduction model for the prediction of convection dominated solid–liquid phase change, Int. J. Heat Mass Transf. 52 (7) (March 2009) 1753–1760.
[49] V.R. Voller, C. Prakash, A fixed grid numerical modelling methodology for convection-diffusion mushy region phase-change problems, Int. J. Heat Mass Transf. 30 (8) (August 1987) 1709–1719.
[50] S. Wang, A. Faghri, T.L. Bergman, A comprehensive numerical model for melting with natural convection, Int. J. Heat Mass Transf. 53 (9) (April 2010) 1986–2000.
[51] Z. Zhang, A. Naga, A new finite element gradient recovery method: superconvergence property, SIAM J. Sci. Comput. 26 (4) (2005) 1192–1213.
[52] A.G. Zimmerman, J. Kowalski, Monolithic simulation of convection-coupled phase-change - verification and reproducibility, arXiv:1801.03429, 2018.
[53] A.G. Zimmerman, J. Kowalski, Simulating Convection-Coupled Phase-Change in Enthalpy Form with Mixed Finite Elements, 2019.